Angle-resolved photoemission spectroscopy of the metallic sodium tungsten bronzes Na_xWO_3

S. Raj,* D. Hashimoto, H. Matsui, S. Souma, T. Sato, and T. Takahashi
Department of Physics, Tohoku University, Sendai 980-8578, Japan

Sugata Ray, A. Chakraborty, and D. D. Sarma†
Solid State and Structural Chemistry Unit, Indian Institute of Science, Bangalore 560 012, India

Priya Mahadevan
Department of Physics, Indian Institute of Technology, Chennai 600 036, India

W. H. McCarroll
Department of Chemistry and Biochemistry, Rider University, Lawrenceville, New Jersey 08648, USA

M. Greenblatt
Department of Chemistry and Chemical Biology, The State University of New Jersey, Piscataway, New Jersey 08854, USA

We have carried out high-resolution angle-resolved photoemission spectroscopy (ARPES) to study the electronic structure of highly metallic Na_xWO_3 (x=0.58, 0.65, 0.7, and 0.8). The experimentally determined valence-band structure has been compared with the results of an *ab initio* band-structure calculation. While the presence of an impurity band (level) induced by Na doping is often invoked to explain the insulating state found at low concentrations, we find no signature of impurity band (level) in the metallic regime. The states near E_F are populated and the Fermi edge shifts rigidly with increasing electron doping (x). The linear dispersion of the conduction band explains the linear variation of thermodynamic properties including the specific heat and magnetic susceptibility. The presence of an electron-like Fermi surface at $\Gamma(X)$ and its evolution with increasing Na content and the rigid shift of the Fermi level with increasing x agrees well with the band calculation.

I. INTRODUCTION

The studies of tungsten-oxide-based materials are of enormous interest in material science as a result of various applications. Stoichiometric bulk WO_3 is yellowish-green and monoclinic at room temperature. It is possible to insert sodium (Na) in WO_3, thus forming the series Na_xWO_3; the color changes from yellowish-green to gray, blue-deep-violet, red, and finally to gold as x increases from zero to unity.[1] WO_3 modified by ion incorporation or substoichiometry exhibits many technologically important properties.[2,3] Na_xWO_3 exhibits interesting electronic properties, especially a metal-insulator transition (MIT) as a function of x. A high-metallic conduction is obtained for $x \geqslant 0.25$, while the system undergoes MIT with decreasing x. Hence, the study of electronic structure of Na_xWO_3 is of great interest from both technological and fundamental perspectives.

The structural evolution[4] of Na_xWO_3 is also interesting to study, since it changes from monoclinic, to orthorhombic, to tetragonal, and finally to cubic with increasing x. For $x \leqslant 0.5$, it exists in a variety of structural modifications, while for $x \geqslant 0.5$, Na_xWO_3 is a metallic continuous solid solution with perovskite-type crystal structure. Brown and Banks[5] have shown that the lattice parameter varies as $a=3.7845+0.0820x$(Å) for highly metallic Na_xWO_3. Figure 1(a) shows the crystal structure of $NaWO_3$. In Na_xWO_3, Na ions occupy the center of the cube, while the W ions are located at the cube corners. The oxygens are at the edge centers and, therefore, form WO_6 octahedra with each W ion. The octahedral crystal field of the six oxygen neighbors of the W split the W $5d$ bands into triply degenerate t_{2g} and doubly degenerate e_g bands (in the cubic phase, when the WO_6 octahedra are distorted, the degeneracy of these levels may be further split by the lowering of the symmetry). In WO_3, the Fermi level (E_F) lies at the top of the O p bands, and WO_3 is a band insulator. Within a rigid-band model, the band structure of both WO_3 and $NaWO_3$ should be identical with E_F at different positions. In Na_xWO_3, the Na $3s$ electrons are transferred into the W $5d$ t_{2g} band and the system becomes metallic for $x \geqslant 0.25$.[6] However, for low concentration of $x(x \leqslant 0.25)$ the material is insulating; the origin of the MIT is still under debate. According to the Anderson localization model,[7] the random distribution of Na^+ ions in the WO_3 lattice gives rise

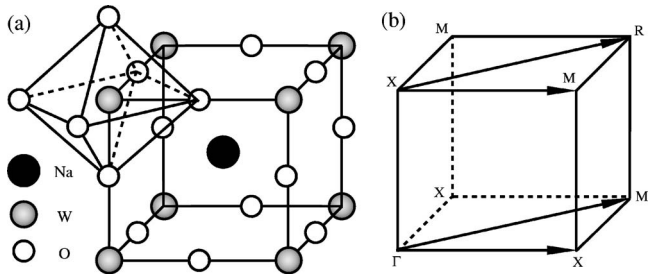

FIG. 1. (a) Crystal structure of $NaWO_3$ and (b) cubic Brillouin zone of $NaWO_3$ showing high-symmetric lines.

to strong disorder effects that lead to the localization of states in the conduction band tail. The system undergoes a MIT for low Na concentration. An alternative explanation for the MIT is the development of an impurity band (level) induced by Na doping, where the states become localized at low Na concentration. Another possibility driving the MIT is the splitting of the band at the chemical potential (or E_F) into two bands: the upper Hubbard band (UHB) and the lower Hubbard band (LHB),[8] where the localization occurs in a pseudogap between the two bands. However, the Hubbard gap would coincide with the chemical potential (or E_F) only if the band were half filled, which is unlikely in the context of Na_xWO_3. Among the various models proposed to explain the MIT in Na_xWO_3, Anderson localization seems to be the most appropriate one.

Many photoemission studies[9–12] have been reported on Na_xWO_3 and Höchst *et al.*[13] have performed angle-resolved photoemission spectroscopy (ARPES) on a metallic $Na_{0.85}WO_3$ single crystal with poor energy and momentum resolution. There are conflicting reports on the mechanisms of MIT as mentioned above in many of the previous studies.[9–11] The evolution of electronic structure with x in the metallic regime is also not clear from the previous angle-integrated photoemission studies.[9–11] Moreover, it is difficult to compare the experimental result with band calculations[14–16] due to the poor energy and angular resolution of the experimental data. High-resolution ARPES is necessary to experimentally establish the band structure, evolution of electronic structure with Na doping x, and to clarify the development of an impurity band (level), which is one of the mechanisms proposed for the MIT in Na_xWO_3.

In this paper, we report high-resolution ARPES on highly metallic Na_xWO_3 (x=0.58, 0.65, 0.7, and 0.8). The valence-band structure, as well as the Fermi surface (FS) have been determined experimentally. We have also carried out *ab initio* band-structure calculations based on the plane-wave pseudopotential method and compared the calculated results with experiment. We did not find any impurity band (level) in our band mapping, which is one of the possible mechanisms to explain the observed MIT in Na_xWO_3. The Fermi surface shows an electron-like pocket centered at the $\Gamma(X)$ point in the Brillouin zone [Fig. 1(b)], in good agreement with the band calculation. The volume of Fermi surface monotonically increases with x from 0.58 to 0.8, indicating that Na 3s electrons go to the W 5d t_{2g} conduction band and the states near E_F are filled with Na doping. We find that a simple, rigid band shift of the features can explain the x-dependent band structure in highly metallic Na_xWO_3, where the doped electrons merely fill up the conduction band.

II. EXPERIMENTS

Cubic single crystals of Na_xWO_3 (x=0.58, 0.65, 0.7, and 0.8) were grown by the fused salt electrolysis of Na_2WO_4 and WO_3 as described by Shanks.[17] The resistivity measurements and Laue diffraction pattern show that the crystals are metallic with a single cubic phase, respectively. The x values were obtained from the measured lattice parameters as described by Brown and Banks.[5] ARPES measurements were performed with a GAMMADATA-SCIENTA SES 200 spectrometer with a high-flux discharge lamp and a toroidal-grating monochromator. The He Iα ($h\nu$=21.218 eV) resonance line was used to excite photoelectrons. The energy and angular (momentum) resolutions were set at 5–11 meV and 0.2°(0.01 Å^{-1}), respectively. The measurements were performed at 14 K in a vacuum of 3×10^{-11} Torr base pressure. A clean surface for photoemission measurements was obtained by *in situ* cleaving. After each set of measurements, we checked the degradation of the sample surface by checking the background of the spectrum and found no degradation to the surface. The Fermi level (E_F) of the sample was referred to that of a gold film evaporated on the sample substrate.

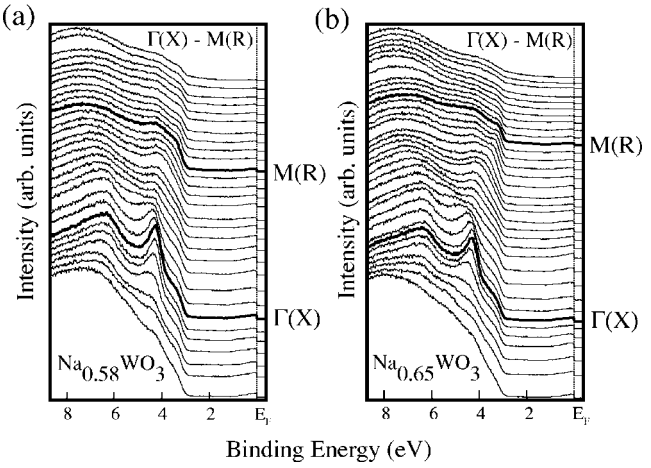

FIG. 2. Valence-band ARPES spectra of (a) $Na_{0.58}WO_3$ and (b) $Na_{0.65}WO_3$ measured at 14 K with He-Iα photons (21.218 eV) along the $\Gamma(X)$-$M(R)$ direction of Brillouin zone.

III. BAND CALCULATIONS

We have performed *ab initio* band-structure calculations using projected-augmented wave potential[18,19] as implemented in the VASP code.[20] A **k**-points mesh of $8\times8\times8$, lattice constant of 3.85 Å, and the generalized-gradient approximation for the exchange was used for the calculation. We have simulated electron doping in our calculations by a rigid band shift of the band structure. The Fermi surfaces have been calculated for different concentrations.

IV. RESULTS AND DISCUSSION

A. Valence-band region

Figure 2 shows the valence-band ARPES spectra of Na_xWO_3 for x=0.58 and 0.65, measured at 14 K with He Iα photons along the $\Gamma(X)$-$M(R)$ high-symmetry line in the cubic Brillouin zone. In Na_xWO_3, the Fermi level is situated in the conduction band and the bottom of the conduction band extends up to nearly 1.0 eV binding energy as seen in Fig. 2. The top of the valence band extends up to 3.0 eV binding energy. There is a large (~2 eV) energy gap between the bottom of the conduction band and the top of the valence

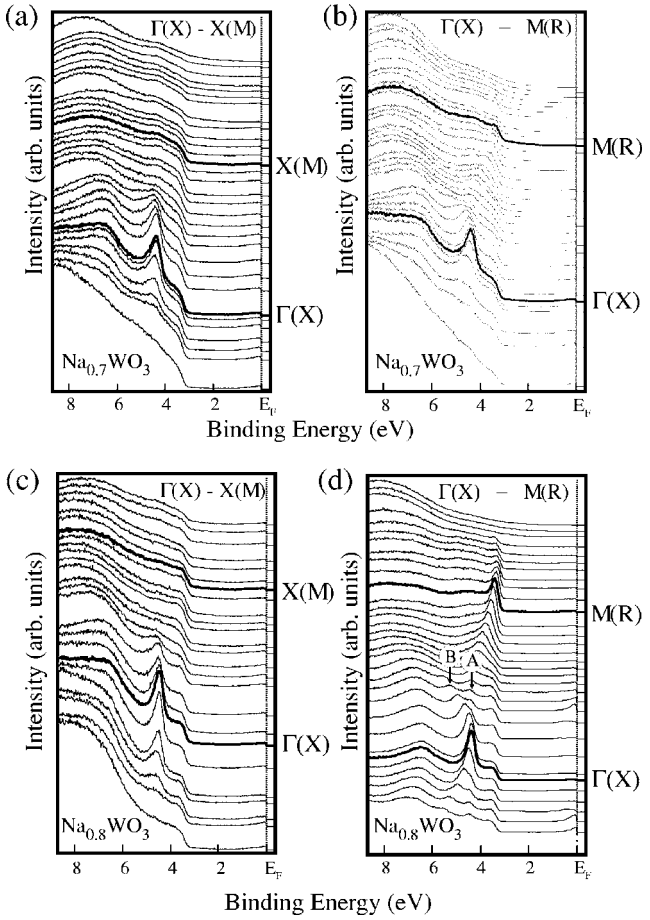

FIG. 3. Valence-band ARPES spectra of $Na_{0.7}WO_3$ (a) along $\Gamma(X)$-$X(M)$ and (b) along $\Gamma(X)$-$M(R)$ and of $Na_{0.8}WO_3$ (c) along $\Gamma(X)$-$X(M)$ and (d) along $\Gamma(X)$-$M(R)$ of Brillouin zone, measured at 14 K with He-Iα photons (21.218 eV).

band. The spectral features of Na_xWO_3 for x=0.58 and 0.65 look essentially the same. A clear Fermi edge is visible in these metallic compounds. The intensity near E_F at $\Gamma(X)$ is gradually reduced while moving toward $M(R)$. There are three prominent peaks visible around the $\Gamma(X)$-$M(R)$ direction. A nondispersive peak at 3.3 eV at $\Gamma(X)$ gradually loses its intensity while moving toward $M(R)$ and once again becomes prominent around $M(R)$. The most prominent peak in the valence band is seen at 4.3 eV at $\Gamma(X)$ and disperses downward around $\Gamma(X)$ along with the decrease of its peak intensity. We observe a broad peak at 6.3 eV around $\Gamma(X)$, which disperses downward by going toward $M(R)$. It is to be noted that another weak feature, away from $\Gamma(X)$, is developing around 5 eV with increasing x. No additional bands are found to emerge in the relevant energy window with Na doping, which suggests that a rigid-band model is adequate.

Figure 3 shows the valence-band ARPES spectra of Na_xWO_3 for x=0.7 and 0.8, measured at 14 K with He Iα photons along both the $\Gamma(X)$-$X(M)$ and $\Gamma(X)$-$M(R)$ high-symmetry lines. We find that all the spectral features are essentially similar in Na_xWO_3 for both x=0.7 and 0.8. However, in $\Gamma(X)$-$X(M)$ direction, the intense peak at 4.3 eV does not disperse as in the $\Gamma(X)$-$M(R)$ direction [see Figs. 3(b) and 3(d)]. The weak spectral feature around 5 eV develops clearly when the Na concentration increases to 0.8. We clearly see four peaks near $\Gamma(X)$ point [Fig. 3(d)]. Two peaks between 4 and 6 eV marked as A and B merge to a single intense peak at 4.3 eV around $\Gamma(X)$. The peak marked B highly disperses downward while moving away from $\Gamma(X)$ and merges with the 6.3 eV peak, whereas the peak marked as A slowly disperses to lower-binding energy. With increasing Na concentration in Na_xWO_3, all the peaks become more intense and sharper as contrasted in Figs. 2(a) and 3(d). This is attributed to the decrease of disorder in the system.

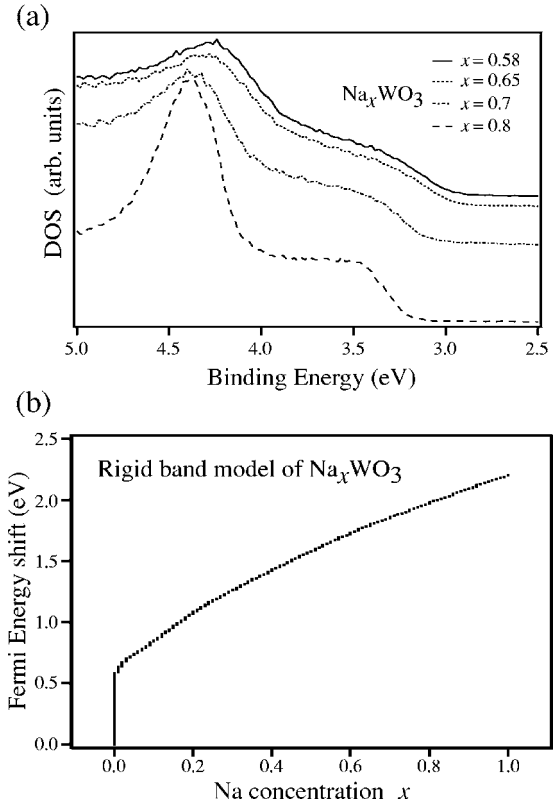

FIG. 4. (a) Comparison of ARPES spectrum near valence-band edge in Na_xWO_3 for x=0.58, 0.65, 0.7, and 0.8. (b) Calculated Fermi energy shift with Na doping x from the rigid-band model.

In Fig. 4, we show the near-valence band-edge region of the valence-band spectra at $\Gamma(X)$ of the different compositions studied here. A clear shift in the valence-band edge is seen as the Na content is increased. We have shifted the spectra (after normalizing the area under the curve), superimposed them, and determined the shift to be $\sim$0.24 eV as x is varied from 0.58 to 0.8. Figure 4(b) shows the theoretically computed energy shift calculated from a rigid-band model. The experimental shift (0.24 eV) is quite close to the theoretically computed shift of $\sim$0.3 eV.

We have mapped out the band structure of Na_xWO_3 for x=0.58 and 0.65 along the $\Gamma(X)$-$M(R)$ direction in Figs. 5(a) and 5(b), respectively. The experimental band structure has been obtained by taking the second derivative of the ARPES spectra and plotting the intensity by gradual shading as a function of the wave vector and the binding energy. The bright areas correspond to the experimental bands. We also

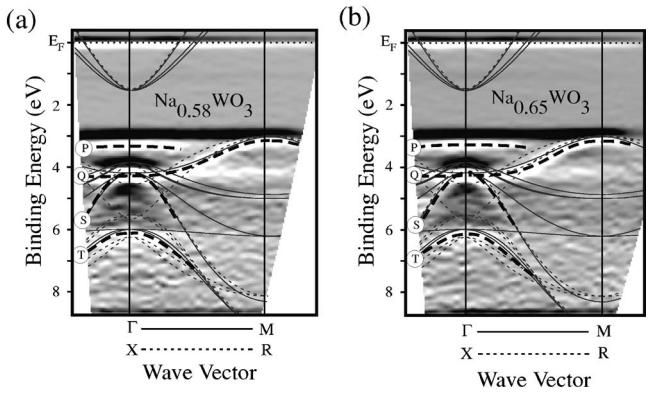

FIG. 5. Experimental valence-band structure of (a) $Na_{0.58}WO_3$ and (b) $Na_{0.65}WO_3$ obtained from the ARPES experiment along the $\Gamma(X)$-$M(R)$ direction. Bright areas correspond to the experimental bands and dark, dashed lines are guides to the experimental bands. Theoretical band structure of $NaWO_3$ based on the plane-wave pseudopotential method is also shown by thin, solid and dashed lines for comparison.

show the pseudopotential band structure of cubic $NaWO_3$ for comparison as thin, solid and dashed lines. In both Figs. 5(a) and 5(b), we clearly see primarily four bands (bands P, Q, S, and T as shown with dark, dashed lines) in the valence band region. Theoretical band calculation predicts parabolic bands which are located around the $\Gamma(X)$ point and cross the Fermi level as shown in Fig. 5. In experimental band mapping, the intensity of these bands are very small compared to the higher-binding energy bands (especially band Q). Hence, the intensity of near-E_F bands are not clearly visible as we use the gradual shading of the second derivative of the ARPES intensity. But we clearly see the band dispersion in near-E_F band mapping, which we have described in a later part of this article. The experimental band structures are essentially similar for both $x=0.58$ and 0.65 along the $\Gamma(X)$-$M(R)$ direction. The top of the valence band (band P) at 3.3 eV binding energy around $\Gamma(X)$ is not predicted in the band calculation. This apparently flat band may be dominated by the angle-integrated-type background from the strong intensity of band Q at the $M(R)$ point. The dispersion of band Q around 4.3 eV binding energy at $\Gamma(X)$ and another band S, which disperses highly downward from $\Gamma(X)$ to $M(R)$ are in good agreement with the band calculation. The intensity along the $\Gamma(X)$-$M(R)$ direction at 4.3 eV arises due to angle-integrated-type background arising due to finite-electron scattering from the strong intensity of bands Q and S at $\Gamma(X)$ and vanishes with the decrease of disorder in Na_xWO_3 (for $x=0.7$ and 0.8 disorder is less; hence, the effect is not clearly visible). This flat band raises questions on the homogeneity of the samples; hence, we have carried out various measurements to ensure the homogeneity of the samples for all the compositions studied here. The x-ray diffraction (XRD) pattern of the single crystals shows that the samples are good quality without impurity. The energy dispersive x-ray analysis (EDAX) measurements also do not show any inhomogeneity within the instrument resolution. Now, repeated charge-coupled device (CCD) XRD (however, CCD XRD is nothing but single-crystal diffraction experiments in which the data

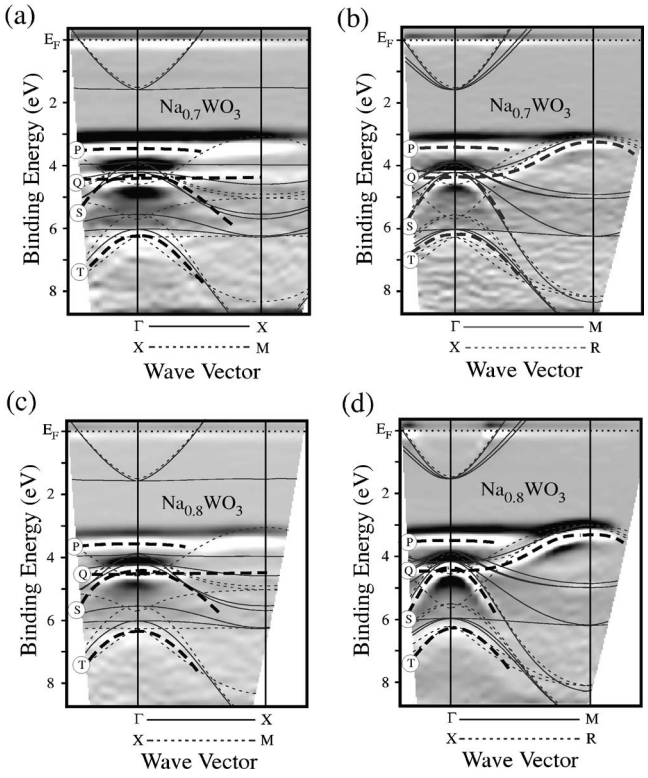

FIG. 6. Experimental valence-band structure of $Na_{0.7}WO_3$ (a) along $\Gamma(X)$-$X(M)$ and (b) along $\Gamma(X)$-$M(R)$ and of $Na_{0.8}WO_3$ (c) along $\Gamma(X)$-$X(M)$ and (d) along $\Gamma(X)$-$M(R)$ direction. Bright areas correspond to the experimental bands and dark, dashed lines are guide to the experimental bands. Theoretical band structure of $NaWO_3$ based on the plane-wave pseudopotential method is also shown by thin, solid and dashed lines in respective high-symmetry directions for comparison.

are collected simultaneously from many angles and, therefore, the collection time is short) measurements on our samples showed that the crystals are of good quality (with sharp spot intensities), without any defect (like twin boundaries, etc.), and devoid of any impurity (no extra spots are found and the pattern in all could be matched with the standard cubic structure of metallic Na_xWO_3). Hence, we conclude that the flat band is arising from angle-integrated background due to the presence of finite disorder in the samples. From the band calculation, we assign the broad band T at 6.3 eV to a group of highly dispersive bands. The gross features of the experimental valence band at higher-binding energy (4–8 eV) can be explained by the *ab initio* band-structure calculations. These calculations also show that the valence band (3–9 eV) consists of mostly O $2p$ character of Na_xWO_3 with a small admixture of bonding W $5d$ character.

Figure 6 shows the experimental band mapping of Na_xWO_3 for $x=0.7$ and 0.8 along the $\Gamma(X)$-$X(M)$ and $\Gamma(X)$-$M(R)$ high-symmetry lines, together with the *ab initio* band structure. Both band structures for $x=0.7$ and 0.8 along $\Gamma(X)$-$X(M)$ and $\Gamma(X)$-$M(R)$ are essentially similar. In both compositions, we find two, flat nondispersive bands (marked P and Q) at 3.5 and 4.5 eV around $\Gamma(X)$ along the $\Gamma(X)$-$X(M)$ direction. The energy position of the experimental bands does not agree well with the band calculation, al-

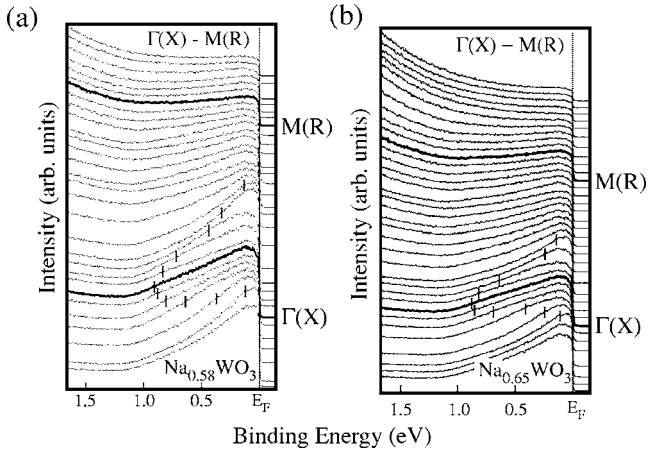

FIG. 7. ARPES spectra near E_F of (a) $Na_{0.58}WO_3$ and (b) $Na_{0.65}WO_3$ measured at 14 K with He-Iα photons (21.218 eV) along the $\Gamma(X)$-$M(R)$ direction. Vertical bars are a guide to the eye for band dispersion.

though the band calculation predicts a flat band along the $\Gamma(X)$-$X(M)$ direction. The band structures along the $\Gamma(X)$-$M(R)$ direction for x=0.7 and 0.8 are similar to those of x =0.58 and 0.65, showing four dispersive bands in the valence-band region. Comparison of valence-band structures of x=0.58 and 0.8 shows that all the bands in the valence-band regime move downward rigidly. Thus, with increasing x in Na_xWO_3, the Na 3s electrons just fill the W 5d t_{2g} conduction band and change the E_F position consistent with the rigid-band model appropriate for the compositions studied here.

B. Near-E_F region

In order to study the electronic structure near E_F in more detail, we have carried out high-resolution ARPES measurements with a smaller energy interval and a higher signal-to-noise ratio. Figures 7 and 8 show the high-resolution ARPES spectra near E_F of Na_xWO_3 for x=0.58, 0.65, 0.7, and 0.8 measured at 14 K with He Iα photons along the high-symmetry directions in the Brillouin zone. We observe a very weak broad feature near 0.9 eV at $\Gamma(X)$, which disperse upward to form an electron-like pocket at $\Gamma(X)$ for all compositions of x. There is no signature of such a feature at $X(M)$ or $M(R)$. As the Na concentration increases, this feature becomes very prominent as shown in Fig. 8(d). This behavior may be due to the decrease of disorder with increasing x in the system. In both figures, the bottom of the conduction band lies roughly around 0.9–1.0 eV below E_F. The exact position of the band bottom is difficult to determine due to the very low spectral intensity at the band bottom; nevertheless, it is clear that the conduction band bottom moves downward with Na concentration similar to the trend seen for the valence band. This can be explained by considering the simple rigid-band shift. Since the determination of the exact position of the band bottom has much more ambiguity, it is difficult to determine quantitatively the shift of the band bottom from x=0.58 to 0.8. Previous reports[13,21–23] that the bandwidths of occupied conduction states appear to be almost independent of Na concentration are not supported by our results. Since the density of states (DOS) at band bottom is very low and the background is high, it is impossible to get the exact bandwidths of occupied states from the previous angle-integrated measurements.

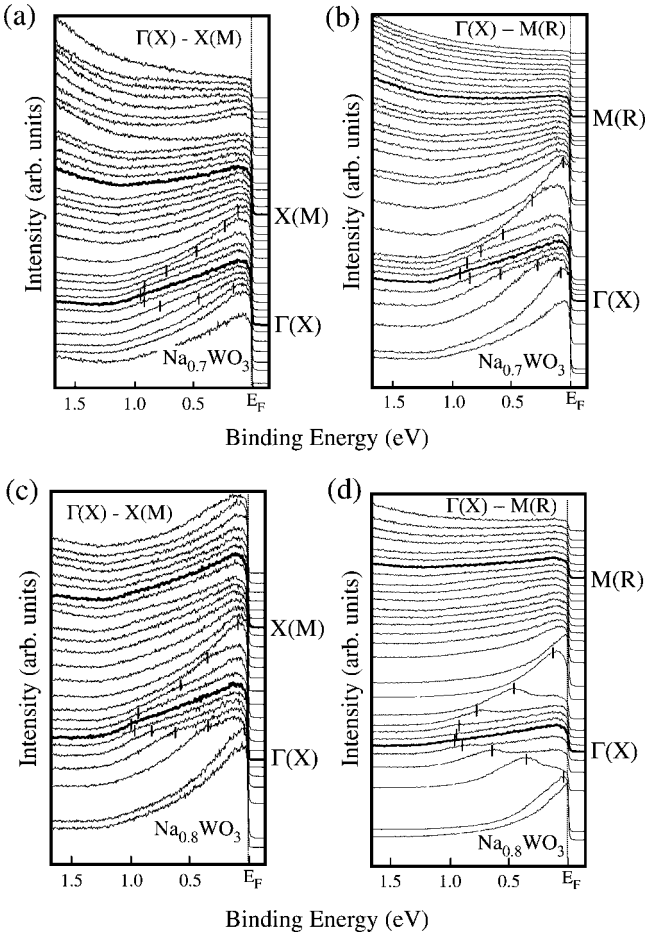

FIG. 8. ARPES spectra near E_F of $Na_{0.7}WO_3$ (a) along $\Gamma(X)$-$X(M)$ and (b) along $\Gamma(X)$-$M(R)$ and of $Na_{0.8}WO_3$ (c) along $\Gamma(X)$-$X(M)$ and (d) along $\Gamma(X)$-$M(R)$ direction, measured at 14 K with He-Iα photons (21.218 eV). Vertical bars are a guide to the eye for band dispersion.

Figure 9 shows the plot of ARPES intensity as a function of the wave vector and the binding energy, showing the experimental band structure near E_F. We find an electron-like pocket at $\Gamma(X)$, whose linear dispersion at E_F agrees satisfactorily with the band calculation. We find a clear variation in the spectral intensity at E_F, which suggests that the band crosses E_F at the highest intensity. Though our present study on different compositions are far from MIT regime, we believe that if the impurity band and/or level would be the cause of MIT, then it should have signature in metallic regime though the impurity band and/or level would have lain much below the Fermi level. But no such signature of the impurity band (level) near E_F is seen in Fig. 9 except W 5d bands, which rules out the development of a Na-induced impurity band (level). Hence, we conclude that the previous speculation regarding MIT at low Na concentration being due to the development of Na-induced impurity band (level) is not supported by our results.

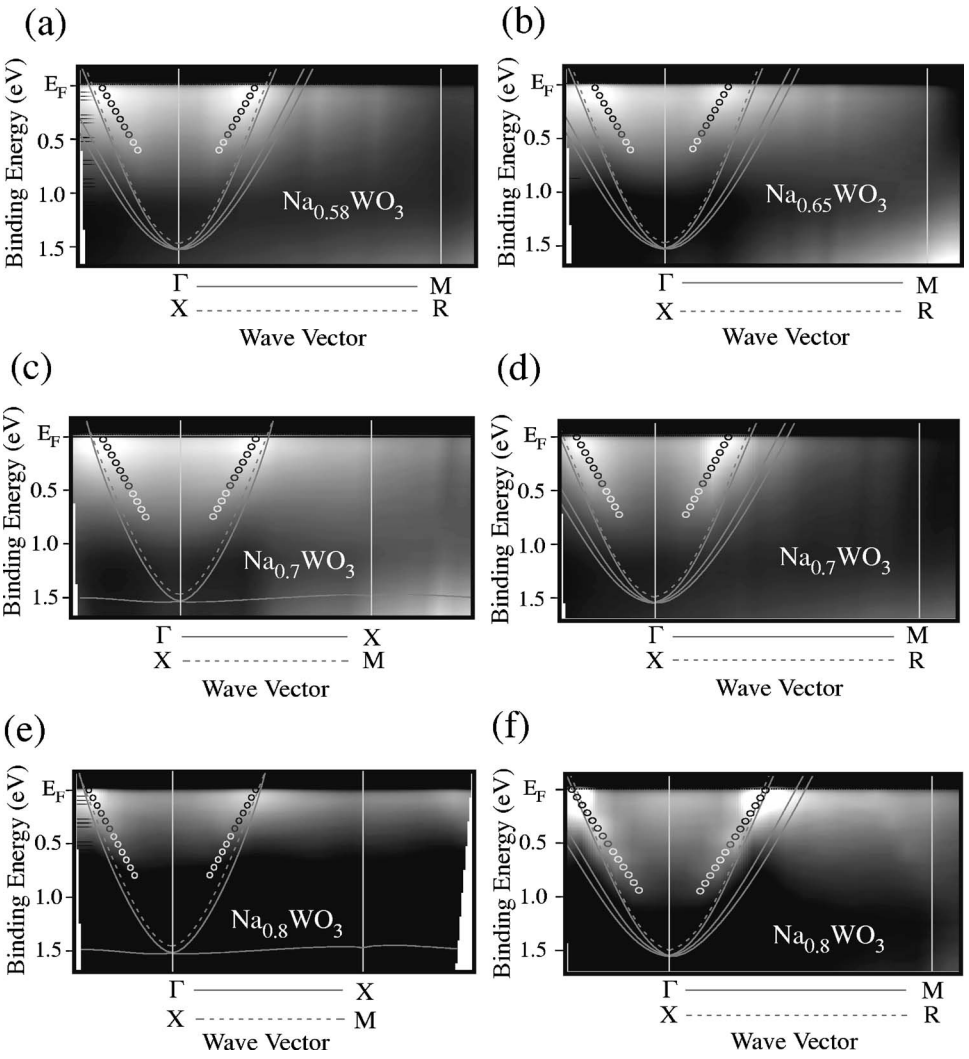

FIG. 9. Experimental near-E_F band structure of (a) $Na_{0.58}WO_3$ along $\Gamma(X)$-$M(R)$, (b) $Na_{0.65}WO_3$ along $\Gamma(X)$-$M(R)$, $Na_{0.7}WO_3$ (c) along $\Gamma(X)$-$X(M)$ and (d) along $\Gamma(X)$-$M(R)$, and $Na_{0.8}WO_3$ (e) along $\Gamma(X)$-$X(M)$ and (f) along $\Gamma(X)$-$M(R)$ direction. Theoretical band structure of $NaWO_3$ is also shown by thin, solid and dashed lines for comparison. Open circles show the highest intensity in experimental band mapping.

In the rigid-band model with a spherical Fermi surface and rigid parabolic density of states, the density of states N(E) is proportional to $E^{1/2}$. It is assumed that all sodium atoms are ionized in Na_xWO_3; hence, N(E_F), the density of states at E_F, is proportional to $x^{1/3}$. However, the physical properties including the magnetic susceptibility and the specific heat coefficient[24] γ were found to vary linearly with x. We extrapolated the band dispersion from the highest intensity points of the band mapping (shown as open circles in Fig. 9) and find that the conduction bandwidth expands with increasing x; the experimental band dispersion is not a free electron-like parabolic as proposed before. The *ab initio* band structure results also show linear band dispersion as observed experimentally. The expansion of the conduction band can be well explained by the linear increase in the density of states of the conduction band with increasing x in Na_xWO_3. This explanation fits well with the x-dependent behavior of the specific heat and the magnetic susceptibility, which vary linearly with x for cubic, metallic Na_xWO_3. The heat capacity data[24] show that the effective mass ($m^\star$) of conduction electrons increase monotonically with x. We determined the effective mass from the Fermi velocity v_F at E_F and found a similar monotonic increase in the effective mass of the conduction electrons for all x values studied here. The band mass is less than the free-electron mass m_0 and agrees well quantitatively with the mass found from other experiments.[25]

C. Fermi surface topology

In Fig. 10, we show the ARPES-intensity plot at E_F for Na_xWO_3 (x=0.58, 0.7, and 0.8) as a function of the two-dimensional (2D) wave vector. The intensity is obtained by integrating the spectral weight within 20 meV with respect to E_F and symmetrized with the cubic symmetry. We have also calculated the FS(s) (on ΓXMX and $XMRM$ plane) for fractional Na concentration in Na_xWO_3 assuming rigid band shifts, which are shown by dotted lines. We observe one spherical electron-like Fermi surface centered at the $\Gamma(X)$ point, which is covered with another square-like Fermi surface. Along the $\Gamma(X)$-$X(M)$ direction, we find only one k_F point; while along the $\Gamma(X)$-$M(R)$ direction, there are two distinct k_F points. These two Fermi surfaces are attributed to the W 5d t_{2g} bands. On increasing the Na concentration, the Na 3s electrons are transferred to the W 5d t_{2g} band at E_F. Hence, the volume of the FS gradually increases in accordance with the increase of the Na concentration. The 2D area of the FS at $\Gamma(X)$ is estimated to be 11.5±2% of the whole

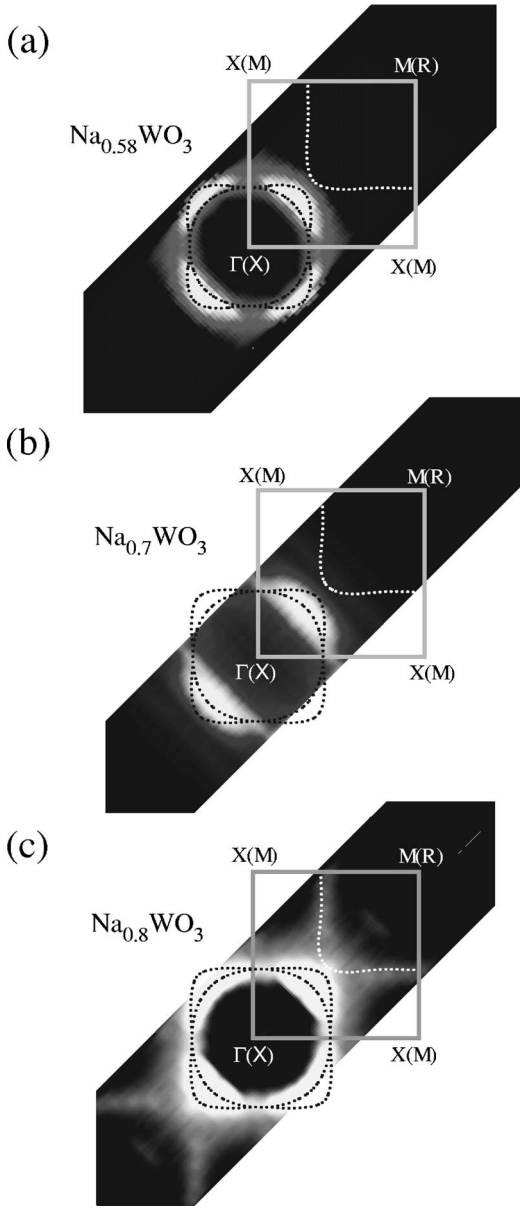

FIG. 10. Fermi surfaces of (a) $Na_{0.58}WO_3$, (b) $Na_{0.7}WO_3$, and (c) $Na_{0.8}WO_3$ showing electron-like pocket at $\Gamma(X)$ point. Dotted lines at $\Gamma(X)$ point are the calculated FS(s) (on ΓXMX and $XMRM$ plane) for fractional Na concentration based on the rigid-band model.

ΓXMX Brillouin-zone 2D plane in $Na_{0.58}WO_3$ and increases to 16.8±2% in $Na_{0.8}WO_3$ [see Fig. 10(c)]. Whereas, we found the calculated 2D area of FS of $NaWO_3$ at $\Gamma(X)$ to be 22% of the whole ΓXMX Brillouin-zone plane. The square-like FS centered at the M point is not clearly visible in Na_xWO_3 for $x=0.58$ and 0.7, but is prominent in $x=0.8$. This FS arises from one single band, whereas the FS(s) observed at $\Gamma(X)$ are from three bands (two from ΓXMX and one from the $XMRM$ planes); hence, the intensity is much more enhanced around $\Gamma(X)$ in the ARPES experiment. The volume of calculated FS and experimental FS matches well for all compositions studied here. A rigid shift of the Fermi energy is found to give a qualitatively good description of the Fermi surface.

V. CONCLUSION

We have carried out high-resolution angle-resolved spectroscopy on highly metallic Na_xWO_3 for $x=0.58$, 0.65, 0.7, and 0.8. We have experimentally determined the valence-band structure and compared it with the *ab initio* band-structure calculations. From the comparison of the experimental band structure of $Na_{0.58}WO_3$ and $Na_{0.8}WO_3$, we concluded that the rigid shift of band structure can explain the metallic Na_xWO_3 band structure with respect to Na doping. We did not observe any signature of impurity band (level) near E_F, and hence, the possibility of development of Na-induced impurity band (level) is ruled out. We observed linear band dispersion near E_F, which shows that the conduction band is not a free electron-like parabolic band. The band mass increases linearly and well explains the linear behavior of thermodynamic properties with increasing Na doping. We observed electron-like FS at the $\Gamma(X)$ point as predicted from band calculation and the FS gradually increases with increasing Na concentration due to W $5d$ t_{2g} band filling. A rigid shift of the Fermi energy is found to give a qualitatively good description of the Fermi surface.

ACKNOWLEDGMENTS

This work is supported by grants from the JSPS and the MEXT of Japan. S. Raj thanks the 21st century COE program "Exploring new science by bridging particle-matter hierarchy" for financial support. H.M. and S.S. acknowledge financial support from JSPS. The work of W.H.McC. and M.G. was supported by Grant No. NSF-DMR-0233697.

*Corresponding author.
Electronic address: raj@arpes.phys.tohoku.ac.jp
†Also at Jawaharlal Nehru Centre for Advanced Scientific Research, Bangalore 560 054, India.

[1] J. B. Goodenough, in *Progress in Solid State Chemistry*, edited by H. Reiss (Pergamon, Oxford, UK, 1971), Vol. 5, pp. 145–399.
[2] C. G. Granqvist, *Handbook of Inorganic Electrochromic Materials* (Elsevier, Amsterdam, 1995).
[3] P. M. S. Monk, R. J. Mortimer, and D. R. Rosseinsky, *Electrochromism: Fundamentals and Applications* (VCH Verlagsgesellschaft, Weinheim, 1995).
[4] A. S. Ribnick, B. Post, and E. Banks, *Non-Stoichiometric Compounds*, Advance in Chemistry Series (American Chemical Society, Washington, DC, 1963), Vol. 39, p. 246.
[5] B. W. Brown and E. Banks, J. Am. Chem. Soc. **76**, 963 (1954).
[6] H. R. Shanks, P. H. Slides, and G. C. Danielson, *Non-Stoichiometric Compounds*, Advance in Chemistry Series (American Chemical Society, Washington, DC, 1963), Vol. 39,

p. 237.
[7] P. W. Anderson, Phys. Rev. **109**, 1492 (1958).
[8] N. F. Mott, *Metal-Insulator Transitions* (Taylor and Francis, London, 1990).
[9] R. L. Benbow and Z. Hurych, Phys. Rev. B **17**, 4527 (1978).
[10] M. D. Hill and R. G. Egdell, J. Phys. C **16**, 6205 (1983).
[11] G. Hollinger, P. Pertosa, J. P. Doumerc, F. J. Himpsel, and B. Reihl, Phys. Rev. B **32**, 1987 (1985).
[12] T. Wolfram and L. Sutcu, Phys. Rev. B **31**, 7680 (1985).
[13] H. Höchst, R. D. Bringans, and H. R. Shanks, Phys. Rev. B **26**, 1702 (1982).
[14] L. Koop, B. N. Harmon, and S. H. Liu, Solid State Commun. **22**, 677 (1977).
[15] N. E. Christensen and A. R. Mackintosh, Phys. Rev. B **35**, 8246 (1987).
[16] M. G. Stachiotti, F. Corà, C. R. A. Catlow, and C. O. Rodriguez, Phys. Rev. B **55**, 7508 (1997).
[17] H. R. Shanks, J. Cryst. Growth, **13/14**, 433 (1972).
[18] P. E. Blöchl, Phys. Rev. B **50**, 17953 (1994).
[19] G. Kresse and D. Joubert, Phys. Rev. B **59**, 1758 (1999).
[20] G. Kresse and J. Furthmüller, Phys. Rev. B **54**, 11169 (1996); Comput. Mater. Sci. **6**, 15 (1996).
[21] M. Campagna, G. K. Wertheim, H. R. Shanks, F. Zumsteg, and E. Banks, Phys. Rev. Lett. **34**, 738 (1975).
[22] H. Höchst, R. D. Bringans, H. R. Shanks, and P. Steiner, Solid State Commun. **34**, 41 (1980).
[23] G. K. Wertheim and J. N. Chazalviel, Solid State Commun. **40**, 931 (1981).
[24] F. C. Zumsteg, Phys. Rev. B **14**, 1406 (1976).
[25] M. Kielwein, K. Saiki, G. Roth, J. Fink, G. Paasch, and R. G. Egdell, Phys. Rev. B **51**, 10320 (1995).